

# SuperWASP-North Extra-solar Planet Candidates between $3\text{hr} < \text{RA} < 6\text{hr}$

W.I. Clarkson<sup>1,2</sup>, B. Enoch<sup>1</sup>, C. A. Haswell<sup>1</sup>, A. J. Norton<sup>1</sup>, D.J. Christian<sup>3</sup>,  
 A. Collier Cameron<sup>4</sup>, S.R. Kane<sup>4,5</sup>, K.D. Horne<sup>4</sup>, T.A. Lister<sup>4,6,7</sup>, R.A. Street<sup>3,8</sup>,  
 R. G. West<sup>9</sup>, D. M. Wilson<sup>6</sup>, N. Evans<sup>6</sup>, A. Fitzsimmons<sup>3</sup>, C. Hellier<sup>6</sup>, S.T. Hodgkin<sup>10</sup>,  
 J. Irwin<sup>10</sup>, F.P. Keenan<sup>3</sup>, J. P. Osborne<sup>9</sup>, N.R. Parley<sup>1</sup>, D.L. Pollacco<sup>3</sup>, R. Ryans<sup>3</sup>,  
 I. Skillen<sup>11</sup>, and P.J. Wheatley<sup>12</sup>

<sup>1</sup>*Department of Physics & Astronomy, The Open University, Milton Keynes, MK7 6AA, UK*

<sup>2</sup>*Space Telescope Science Institute, 3700 San Martin Drive, Baltimore, 21218, USA*

<sup>3</sup>*APS Division, Department of Physics and Astronomy, Queen's University Belfast, Belfast, BT7 1NN, UK*

<sup>4</sup>*SUPA, School of Physics & Astronomy, University of St. Andrews, North Haugh, St. Andrews, Fife, KY16 9SS, UK*

<sup>5</sup>*University of Florida, PO Box 112005, 211 Bryant Space Science Center, Gainesville, FL, USA.*

<sup>6</sup>*Astrophysics Group, School of Chemistry & Physics, Keele University, Staffordshire, ST5 5BG, UK*

<sup>7</sup>*Las Cumbres Observatory, 6740B Cortona Drive, CA 93117, USA.*

<sup>8</sup>*Dept. of Physics, Broida Hall, University of California, Santa Barbara, CA 93106-9530, USA.*

<sup>9</sup>*Department of Physics & Astronomy, University of Leicester, Leicester, LE1 7RH, UK*

<sup>10</sup>*Institute of Astronomy, University of Cambridge, Madingley Road, Cambridge, CB3 0HA, UK*

<sup>11</sup>*Isaac Newton Group of Telescopes, Apartado de correos 321, E-3700 Santa Cruz de la Palma, Tenerife, Spain*

<sup>12</sup>*Department of Physics, University of Warwick, Coventry, CV4 7AL, UK*

Accepted 2007 July 27. Received 2007 July 27; in original form 2007 March 2

## ABSTRACT

The Wide Angle Search for Planets (WASP) photometrically surveys a large number of nearby stars to uncover candidate extrasolar planet systems by virtue of small-amplitude lightcurve dips on a  $\lesssim 5$ -day timescale typical of the “Hot-Jupiters.” Observations with the SuperWASP-North instrument between April and September 2004 produced a rich photometric dataset of some  $1.3 \times 10^9$  datapoints from 6.7 million stars. Our custom-built data acquisition and processing system produces  $\sim 0.02$  mag photometric precision at  $V = 13$ .

We present the transit-candidates in the 03h-06h RA range. Of 141,895 lightcurves with sufficient sampling to provide adequate coverage, 2688 show statistically significant transit-like periodicities. Of these, 44 pass visual inspection of the lightcurve, of which 24 are removed through a set of cuts on the statistical significance of artefacts. All but 4 of the remaining 20 objects are removed when prior information at higher spatial-resolution from existing catalogues is taken into account. Of the four candidates remaining, one is considered a good candidate for follow-up observations with three further second-priority targets. We provide detailed information on these candidates, as well as a selection of the false-positives and astrophysical false-alarms that were eliminated, and discuss briefly the impact of sampling on our results.

**Key words:** methods: data analysis – planetary systems – stars: variables: other

## 1 INTRODUCTION

The discovery of radial-velocity variations indicative of a close planetary companion to 51 Peg (Mayor & Queloz 1995) caused a revolution in studies of planetary formation and evolution, as planets were traditionally thought not to exist as close as 0.05 A.U. to the parent star (Pollack 1996).

Subsequent radial-velocity searches have uncovered 248 extrasolar planets (as of this writing)<sup>1</sup> orbiting main-sequence objects (e.g. Udry et al. 2000). Many of these systems comprise a population with periods typically  $< 4\text{d}$  and orbital

<sup>1</sup> <http://exoplanets.eu/catalog.php>

separations of order 0.05 A.U., and this was an early challenge to theories of planet-formation and evolution.

Transits combined with radial-velocity measurements offer the only method to probe the internal structure of the exoplanets as they allow the planetary radius and mass to be determined. 22 transiting extrasolar planets<sup>1</sup> now have reported mass & radius estimates (Charbonneau et al. 2007b; Bakos et al. 2007b submitted; Burke et al. 2007 submitted; Torres et al. 2007<sup>2</sup>), and although the number of systems is still low, the emerging picture is of a “main sequence” of gas-giants along the  $\bar{\rho} \sim 1.0 \text{ g cm}^3$  line at masses  $\gtrsim 1 M_J$ , and a second, more diverse population at lower mass but possibly inflated radius (e.g. Bakos et al 2007a).

Studies of transiting exoplanets are driving current planetary formation and disk-migration theory. Chi-squared fitting of physically-motivated lightcurve models to the transit lightcurve allows joint constraints on the orbital inclination and planetary radius as a fraction of the stellar radius. The inclination estimate from the transit-fitting then allows the planetary mass to be estimated directly from radial-velocity measurements (e.g. Moutou et al. 2006). The accuracy to which the planetary radius itself can be determined is limited both by the photometric precision of the lightcurve and the precision of the stellar-radius determination. The latter is typically the limiting factor for space-based photometry (Brown et al. 2001).

## 2 INSTRUMENTATION AND OBSERVATIONS

### 2.1 Instrumentation

SuperWASP-North (hereafter SW-N) was the first multi-camera WASP instrument to enter operation. Full details can be found in Pollacco et al (2006); we summarise here the features relevant to this work. During 2004, the SW-N facility consisted of five wide-angle ( $7.8^\circ \times 7.8^\circ$  field of view) cameras on a rapid-slew fork-mount that allows overheads (for slew and settling between exposures) to be as short as 30 seconds even for slews  $\gtrsim 8^\circ$ . The  $2048 \times 2048$ -pixel detectors yield a plate-scale  $\simeq 13.7''/\text{pixel}$ , requiring careful consideration of the field location and observation-depth to avoid washout by crowding. In 2004 the detector was unfiltered to maximise throughput, with an instrumental bandpass covering most of the Johnson *VRI* range, with blue and red cutoffs at  $4000 \text{ \AA}$  and  $10,000 \text{ \AA}$  respectively. While the mount pointing error is at most two pixels rms across the sky, a slight misalignment of the instrument polar axis leads to a position-drift of  $\sim 10$  pixels during the night.

### 2.2 Observational Strategy

The WASP survey was planned around a broad-but-shallow approach to maximise planet yield, as this brings three key benefits when searching for exoplanet transits.

<sup>1</sup> including the two transiting exoplanets WASP-1b & WASP-2b, which were discovered in other fields from the 2004 WASP survey (Collier Cameron et al. 2007).

<sup>2</sup> as of this writing, this reference is not yet available on the astro-ph preprint server but can be found at <http://exoplanets.eu/catalog-transit.php>

**(i) - Further Exoplanet Diagnostics:** Detectable planetary transits offer the possibility of probing the atmosphere of the transiting planet. Charbonneau et al. (2006) list seven further constraints that can be made on a transiting planet-star system, but *only* if the parent star is sufficiently bright to allow high enough signal-to-noise, including the setting of upper limits on atmospheric absorption features (Deming et al. 2005b), the setting of constraints on the vertical extent of the atmosphere by atomic species (Vidal-Madjar et al. 2004; Charbonneau et al. 2002), the search for spectroscopic features from the planet itself during secondary eclipse (Richardson et al. 2003) and direct detection of thermal emission from the planet itself (Deming et al 2005a). For the scientific return of transiting exoplanets to be fully realised, then, ground-based transit surveys such as WASP are typically optimised for objects at  $V \lesssim 13$ .

**(ii) - Facility of Follow-Up Observations:** One of the byproducts of the *OGLE* microlensing project was a set of objects showing apparent characteristics of exoplanet occultation ( $P_{orb} \sim 1\text{-}10\text{d}$ , flux removal  $\Delta F/F \sim 1\%$ , event duration  $\sim$ hours; Udalski et al. 2002a-c). Strenuous follow-up spectroscopic observations by several groups (e.g. Bouchy et al. 2005) showed that a high fraction of these objects were astrophysical false-alarms such as grazing-incidence stellar binaries or a large-amplitude variable blended with the brighter target. Dedicated narrow-deep photometric surveys (with e.g. *HST* or the upcoming *Kepler* mission) afford such high coverage and spatial resolution that this class of astrophysical false-alarm can be minimised to high confidence from the photometry alone (to the level where  $< 1$  astrophysical false-positive is expected from the entire survey, e.g. Sahu et al. 2006). For ground-based surveys, however, the astrophysical false-positives will, for the foreseeable future, be a large and important class of candidates; a population study using the 2MASS catalogue suggests an *astrophysical* false alarm to transit ratio of at least 10:1 (Brown 2003); ground-based follow-up observations are thus still essential. At the time of survey planning, consideration of a variety of ground-based photometric observing strategies (in the presence of uncorrelated (“white”) noise; Horne 2003) suggested the SW-N hardware would provide survey statistics competitive with all other existing transit surveys while avoiding excessive crowding at fainter magnitudes. The SW-N limiting magnitude to transits of  $V \sim 13$  (with 30-second exposures) allows follow-up observations to take place with  $\sim 1/10$  the exposure time (or collecting area) as similar observations of *OGLE* candidates (themselves in the range  $15 \leq V \leq 21$ ; Udalski et al. 2002a).

**(iii) - Catalogue-based elimination of Astrophysical False-positives:** With the availability of the USNO-B1.0 (hereafter USNO), Tycho-2 and 2MASS catalogues, multicolour absolute magnitude-estimates already exist at higher spatial resolution than the program variability observations. Tycho-2 is  $\sim 90\%$  complete down to  $V \simeq 11.5$  mag (Høg et al. 2000), while comparison with the Sloan Digital Sky Survey suggests USNO is 97% complete for stars out to  $g' \sim 20$  (roughly Johnson B  $\sim 20$ ; Monet et al. 2003). This allows obvious astrophysical false-positives to be eliminated during analysis of the photometry; for the fields we report here roughly 77% of photometrically-promising candidates are ruled out in this manner before any follow-up observations take place.

Thirty-second snapshots of each field of view are taken in sequences of eight surrounding the Meridian; once the sequence is complete the camera returns to the start of the sequence for the next run. The rapid-slew capability of the mount allows a cadence of  $\simeq 9$  minutes per field. Fields centred at declination  $+23^\circ \leq \delta^\circ \leq +32^\circ$  were generally chosen to provide optimal survey grasp without crowding washout, though with Galactic-plane avoidance some fields at other declinations were sampled (see Pollacco et al. 2006)<sup>2</sup>. As the westernmost field in the group of eight moves to high air-mass, this field is abandoned and a new field added on the east. The net result is a lightcurve with  $\sim 9$ -minute cadence, consisting of roughly 35 frames per night for well-sampled fields. As the sky precesses throughout the year, roughly 60 nights' data are collected for each field for each camera.

### 3 ANALYSIS TECHNIQUES

We outline briefly the analysis techniques used in this project. The reduction and detection procedures are described more fully in Pollacco et al. (2006) and Collier Cameron et al. (2006), see also the companion papers in this series (Christian et al. 2006; Lister et al. 2007; Street et al. 2007).

#### 3.1 Photometry Pipeline

The collaboration has built a fully-automated data reduction pipeline that achieves our goal of obtaining photometric precision of  $\sim 1\%$  for stars with  $V < 13$ . Photometric precision is typically 0.02 mag at  $V = 13$ , with 5 millimag achieved at  $V = 8.5$ . The pipeline uses custom written f77 programs and several STARLINK packages called from shell-scripts; it is thus somewhat portable and uses capabilities already freely available as much as possible. The pipeline itself is described more fully in Pollacco et al. (2006); here we remark on its following relevant features:

- (1) Frame classification and quality-control is performed on the input frames through statistical characterisation of the frame content, with minimal reliance on object headers. Currently  $\sim 85\%$  of frames are accepted for further processing depending on the observing conditions during any given night.
- (2) Running calibrations are produced by optimally weighting the calibration history across a season, including exponentially decreasing weighting with a 14-day timescale to allow for varying dust-patterns on the lens and other systematics which can vary with time. This measurably reduces the systematic scatter in the thermal, flatfield and bias frames.
- (3) By triangle-matching selected detected objects with Hipparcos positions in the Tycho-2 catalogue, a full nine-term plate-solution on the tangent plane is derived, allowing for pointing errors and distortion within the glass of the lens by fitting observed stellar positions directly to their catalogued positions on the sky.

- (4) Objects are detected in the frame at  $> 4\sigma$  above background (using a modified version of *SExtractor*; Bertin & Arnouts 1996). Dedicated f77 routines produce aperture photometry in three concentric apertures of radius 2.5, 3.5 and 4.5 pixels. Lightcurves using the 3.5-pixel aperture are retained for further processing; a variant of the curve-of-growth method of Stetson (1990) is used to affix a blending index to each object based on the flux evolution with aperture size.

- (5) Lightcurves from a given field are processed as an ensemble to fit the transformation from the instrumental magnitude system to the Tycho-2  $V$  bandpass. The data are weighted using inverse variance weights that incorporate, in addition to the formal errors from the pipeline, variance components that quantify the intrinsic variability of each star and the patchiness of extinction across each frame. These additional variances are estimated using the maximum-likelihood method described by Collier Cameron et al (2006). The magnitude zeropoint is determined to a precision of 1-2mmag per frame (Pollacco et al. 2006 and Collier Cameron et al. 2006).

- (6) The photometry is then uploaded to the WASP archive at Leicester University, which allows rapid access to time-series of various quantities for each object, through a custom-written query-language based on SQL.

#### 3.2 Photometric Transit Candidates

At this stage, small systematic trends are still present in the photometry; nevertheless, we store these data in the archive rather than storing detrended data. It was envisaged that detrending routines would improve over time; this approach thus allows the user to apply the latest, best routines at the analysis stage. For the work described here, the generalised linear trend-removal algorithm SYSREM (Tamuz et al. 2005) was employed to remove the remaining systematic trends. Investigation is currently underway to fully characterise these trends for future datasets. Under the nominal observing strategy, 35 frames per night are taken for well-sampled fields, however because not all fields are well-sampled under an automated run (for example a field might have only a few frames taken before dawn), we cannot assume all objects are well-sampled. Objects were selected for further analysis for the transit-search if at least 500 points were recorded over more than 10 nights, with Tycho-2  $V \lesssim 13$ .

The resulting set of lightcurves was subjected to automated application of transit-detection algorithms to isolate the small subset of transit-candidates. Comparison of the Matched-filter (Street et al. 2003), Box Least-Squares (Kovács et al. 2002; hereafter BLS) and Bayesian backend (Aigrain & Favata 2002) techniques suggests BLS is most suited to our purposes (Aigrain & Irwin 2004), so was selected as our main transit-search algorithm. Our own Monte-Carlo simulations of the effectiveness of the transit algorithms when applied to artificial transits over real noise lightcurves from WASP, will be reported elsewhere (Enoch et al. in prep). The BLS algorithm was implemented in a two-stage process. An initial coarse-grid search was made over the period-range ( $0.9 \leq P \leq 5$  days), with the period-range chosen to allow some exploration of period-

<sup>2</sup> The full range of declinations imaged including galactic-plane avoidance is thus ( $+12^\circ < \delta^\circ < +47^\circ$ )

**Table 1.** Field statistics. For each field, we report 1.  $N_{cand}$  - the number of targets selected for the BLS search algorithm, 2.  $N_{hun}$  - the number of candidates passed forward for visual selection, 3.  $N_{vis}$  - the number of candidates passing visual selection (Priority 1 / Priority 2), 4.  $N_{S/N}$  - the number of candidates passing further cuts against short periods, ellipsoidal variations and noise signatures (Priority 1 / Priority 2), 5.  $N_f$  - final number of candidates (Priority 1 / Priority 2).

RA	Dec	Nights	Frames	$N_{cand}$	$N_{hun}$	$N_{vis}$	$N_{S/N}$	$N_f$
0316	+3126	60	1882	6810	162	3/5	1/0	0/1
0317	+2326	60	1885	5942	161	3/1	3/0	0/1
0343	+3126	64	1402	8465	115	0/1	0/0	0/0
0344	+2427	27	607	6037	136	0/0	0/0	0/0
0344	+3944	46	1402	17615	417	0/1	0/1	0/0
0416	+3126	46	1400	11106	231	2/1	1/0	0/0
0417	+2326	46	1357	6241	117	0/0	0/0	0/0
0443	+3126	44	1029	8314	147	2/1	2/0	0/0
0444	+3944	43	1014	20432	368	0/1	0/0	0/0
0516	+3126	43	1008	22406	389	5/5	4/2	1/0
0517	+2326	43	1013	13506	219	1/5	1/4	0/1
0543	+3126	37	524	15021	226	4/3	1/0	0/0
Totals				141895	2688	20/24	13/7	1/3

space beneath the 1-day boundary, while still producing well-sampled lightcurves at the long end of the period range. The period interval is set to ensure distinguishable folded lightcurves, in the sense that when folded on two successive periods in the interval, the resulting phase difference of a given feature between the two lightcurves corresponds to the expected transit width at the longest period searched. The results of this coarse pass were refined by a second, finer pass in which the period spacing is now set so that the phase drift over the entire dataset is less than *half* the expected transit width (Collier Cameron 2006). A typical period spacing would thus be 0.002d for the coarse search and 0.001d for the finer search. For each candidate, fit statistics and parameters of the best-fit transit model at this stage were obtained for the five most significant period detections. Detections were ranked by the fit statistic  $\Delta\chi^2$ , which gives the improvement of the best-fitting transit-model over a flat lightcurve model, and is our adopted proxy for the transit S/N detection.

Filtering of the candidate-list was then applied based on: (i) repetition of a transit-like event, (ii) reduced chi-squared statistic of the best-fit transit model  $\chi^2_v < 3.5$ , (iii) the presence of any gaps in the folded transit lightcurve a factor  $> 2.5$  longer than the transit width - indicative of a fit dominated by sampling gaps, (iv) the signal to noise ratio in the presence of correlated noise (commonly called “red-noise”)  $S_{red}$  (Pont et al. 2006), and (v) the transit to anti-transit ratio  $\Delta\chi^2/\Delta\chi^2_-$ . The latter measures the improvement in fit-statistic  $\Delta\chi^2$  when a transit model consisting of regular intensity dips is fit, scaled by the improvement  $\Delta\chi^2_-$  when an “anti-transit” model consisting of regular flux *brightenings* is fit instead. This statistic can be used to characterise lightcurves with a strong correlated noise component (Burke et al. 2006).

Correlated noise introduces significant systematics which raise the detection threshold for significant periodicities in time-series data. Although well-characterized in several fields in astrophysics (such as X-ray variability studies; e.g. Homer et al. 2001), its relevance to optical searches for exoplanets was not fully appreciated when the ground-based transit surveys were planned, and thus deserves some am-

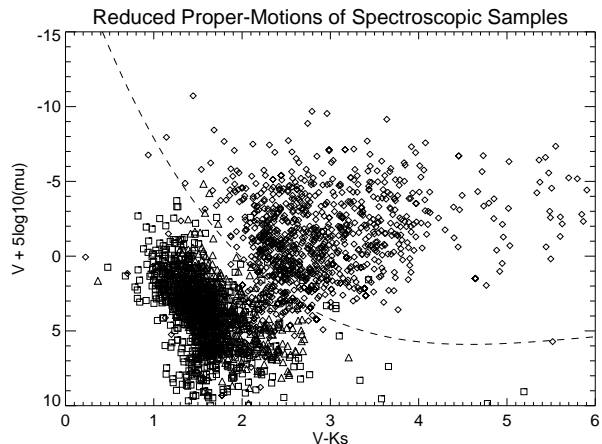


**Figure 1.** Reduced Proper-motion vs  $(V - K_S)$  colour of a selection of giants and dwarfs from the Cayrel et al (2001) and Valenti & Fischer (2005) surveys (using proper motions in  $\text{mas yr}^{-1}$ ). Diamonds: Cayrel et al. giants. Boxes: Cayrel et al. dwarfs. Triangles: Valenti & Fischer dwarfs. The dashed line shows a polynomial boundary (as a function of  $V_{SW} - K_S$ ) constructed to discriminate between the two regions. This boundary serves as a guide for automatic classification, however the position of each photometric transit-candidate was visually checked in this diagram for assessment of luminosity class.

plification here (see also the Discussion, Smith et al. 2006 and Collier Cameron et al. 2006). For ground-based photometric surveys the errors in measurement are usually correlated on timescales of tens of minutes to hours, producing a low-frequency component to the noise that can mimic an exoplanet transit.  $N_{tr}$  transits are observed, with  $L_i$  measurements in each transit. The transit is assumed to be a step-function to the photometric precision of SW-N so that each datapoint observed during transit is treated as an estimate of the full transit depth  $\delta$ . These estimates are binned by transit number, with corresponding binned measurement error  $\sigma_{bin,i}$ . The signal to noise estimate for the full set of

transit measurements is then

$$S_{red}^2 = \sum_{i=1}^{N_{tr}} \frac{\delta_i^2}{\sigma_{bin,i}^2(L_i)} \quad (1)$$

We require a prescription for the relation between binned measurement error  $\sigma_{bin}$  and unbinned error  $\sigma_u$  in the presence of real noise. In the case of SW-N data, this relationship is characterised as

$$\sigma_{bin} = \sigma_u L^b \quad (2)$$

Pure uncorrelated noise would show the familiar  $b = -0.5$  while binning would not improve matters for fully correlated noise and thus  $b = 0$ . For each star, out-of-transit data from each night is used estimate the index  $b$  from a fit to  $\sigma_{bin}/\sigma_u$  as a function of  $L$ . The relation (2) is then used to relate the unbinned rms scatter observed during transit  $\sigma_{u,i}$  to the rms scatter of the binned estimate of the transit depth. In reality,  $L_i$  and  $b$  will vary on a night-by-night basis; in order to filter on a star-by-star basis we take the average across values  $L$  and  $b$  across the observed transits, leading to

$$S_{red} = \frac{\delta\sqrt{N_t}}{\sigma_u L^b} \quad (3)$$

where the rms scatter of the unbinned data  $\sigma_u$  is now taken across all the datapoints during transit. Further information is given in Collier Cameron et al. (2006); note that for objects with  $V < 11$  the covariance parameter  $b$  is not quite -0.5 after detrending, which suggests a low level of residual structure may be present in the detrended lightcurves.

We remind the reader that we are ranking periodicities from each candidate by several criteria in the same search, so care must be taken to interpret the ranking that results. In two cases, the attempt by the algorithm to maximize signal to noise in the presence of correlated noise  $S_{red}$  caused the returned best-fit period to jump to a shorter period that was much less significant than the most significant trough in the BLS periodogram. The  $S_{red}$  statistic can become very low at certain pathological frequencies which beat with the day-night cycle, producing a much higher-than-average number of observable transits. Even if the  $\Delta\chi^2$  is not highly significant at such frequencies,  $S_{red}$  can thus become very large.  $S_{red}$  is therefore only used to determine whether the frequencies associated with the strongest  $\Delta\chi^2$  actually yield significant detections when the contribution from correlated noise is considered.

Detections with the five highest  $S_{red}$  values are produced for each candidates; where the best detections show similar  $S_{red}$  we retained the detection corresponding to the most significant trough in the BLS periodogram (for example the candidate J025922.67+275416.0). In one case the most significant trough in the BLS periodogram only sampled two transits, so we rejected that period and chose the second strongest (J051849.56+211513.6). In most cases, the most significant detection in the BLS periodogram was clearly much more significant than its nearest rivals (see Figure 2) however in at least one case several marginally less significant period-detections were also reported (J051849.56+211513.6; Section 4); no account was taken of these secondary detections in this case.

The result is a set of 2688 transit-candidates ranked by the fit-statistic  $\Delta\chi^2$ . The lightcurves and BLS periodograms for each of these objects were visually examined, to remove

lightcurves dominated by obvious sampling effects and other artefacts. This examination was carried out independently by the first two authors and the final list produced after comparison of the analyses. Objects are deselected from further consideration if their lightcurves meet any two of the following criteria:

1. Folded lightcurve dominated by sampling gaps.
2. Most significantly detected period and the nearest alias of the 1-d sampling are indistinguishable from each other in the BLS periodogram.
3. Visible out-of-transit variability both above and below the mean flux level.
4. Photometric transit-depth,  $\delta$ , greater than 15%.
5. Deep, V-shaped lightcurve suggestive of stellar transit. <sup>2</sup>
6. Ellipsoidal trends apparent in folded lightcurve.
7. Multiple transit events are apparent in the folded lightcurve, suggesting an incorrect period has been used, and the corrected period is outside the 0.9-5 day period range.
8. Transit duration greater than 5 hours.
9. Only two apparent transit events present in the entire lightcurve (if a candidate meets this criteria it is removed from further consideration).

This visual inspection trimmed the 2688 candidates further to 44, comprising 20 targets considered likely from the photometry to contain a transiting extrasolar planet (Priority 1) and 24 candidates where just one of the above tests are failed by the candidates (Priority 2 candidates). At this stage, a number of cuts were made on the surviving objects based on lightcurve statistics returned from the period-search and lightcurve analysis. Objects were only passed forward as candidates if:

1. S/N in the presence of correlated noise  $S_{red} > 8$  (c.f. Pont et al. 2006).
2. Period  $\geq 1.05$  days.
3. S/N of ellipsoidal variations  $< 8.0$  (c.f. Sirko & Paczyński (2003)).
4. Transit to anti-transit ratio  $\Delta\chi^2/\Delta\chi^2_- \geq 2.0$  (c.f. Burke et al. 2006).

All but 20 of the remaining candidates were filtered out by these steps. In summary, then, a typical field would contain several hundred raw candidates, out of which visual inspection would leave 1-2 Priority 1 and 3-4 Priority 2 candidates; however further cuts against correlated noise, ellipsoidal variations and period would reduce this number by about half (see Table 1).

### 3.3 Catalogue-based Assessment

The final cut is the use of prior knowledge from previous surveys with higher spatial resolution and multi-filter information to remove surviving systems that are likely to be blends or other astrophysical false-positives. This stage cut the list of candidates still further.

As we remarked in section 2.2, the depth of the 2MASS,

<sup>2</sup> This criterion was used for objects with  $\gtrsim 10\%$  intensity dips that are clearly stellar binaries; more marginal cases are retained as possible exoplanet candidates.

**Table 2.** Candidates from the BLS search that pass initial visual inspection.  $N_{tr}$  denotes the number of transits observed,  $n_t$  the number of valid observations of the object,  $n$  the number of valid points during transit  $\Delta\chi^2$  the improvement of the best-fitting transit-model over a flat lightcurve model,  $\Delta\chi^2/\Delta\chi_-^2$  the ratio of this fitting statistic when using the transit model to an “anti-transit” brightening model (Section 3.3),  $S_{ell}$  the signal to noise of ellipsoidal variation,  $S_{red}$  the signal to noise including correlated noise. The final two columns give the priority accorded the candidate at the stage of visual examination and the primary reason for its rejection (if applicable). Reasons for removal are: low S/N against correlated “red”-noise (R), presence of ellipsoidal variations (E) and low  $\Delta\chi^2/\Delta\chi_-^2$  (A).

SWASP ID	Period (d)	Duration (hrs)	Depth (mag)	$N_{tr}$	$n_{pts}$	$n$	$\Delta\chi^2$	$\frac{\Delta\chi^2}{\Delta\chi_-^2}$	$S_{ell}$	$S_{red}$	Vis	Cut
J025922.67+275416.0	1.098797	2.38	0.0179	8	1693	129	154.226	2.734	1.051	6.923	P2	R
J025947.03+283310.4	3.074289	4.61	0.0132	5	1694	80	219.119	2.826	3.298	7.335	P2	R
J030117.53+274943.0	3.070961	3.86	0.0241	4	1693	64	103.562	1.661	1.416	6.936	P2	R
J030153.95+332213.0	2.350089	5.18	0.0450	12	1694	228	660.272	4.386	0.399	7.321	P2	R
J031632.80+300144.2	2.198882	3.29	0.0310	6	1692	112	1457.156	5.896	25.784	14.364	P1	E
J032515.17+341031.6	1.011542	3.29	0.0374	17	1693	300	582.241	4.481	6.685	11.121	P1	P
J032739.88+305511.3	1.051158	3.00	0.0253	14	1693	234	911.154	5.764	2.966	9.758	P1	
J033503.83+325915.2	2.135410	2.33	0.0650	9	1694	106	929.219	2.793	15.031	9.837	P2	E
J030157.61+204037.1	1.571295	3.17	0.0807	9	1690	144	2213.008	37.633	3.246	12.431	P1	
J030854.44+234517.4	2.206365	4.25	0.0567	7	1434	101	616.065	8.403	6.469	16.135	P1	
J031103.19+211141.4	2.730148	3.46	0.0403	5	1690	89	712.650	12.847	5.348	9.077	P1	
J033042.00+243027.9	3.178541	3.98	0.0157	3	1690	72	613.552	10.072	11.575	6.354	P2	R
J034747.35+350105.7	1.928731	2.16	0.0254	5	1267	163	2847.39	11.321	13.692	7.533	P2	R
J034628.00+365747.0	1.856870	2.33	0.0703	3	1242	63	736.339	16.640	0.877	8.105	P2	
J041411.76+302105.0	2.554799	4.58	0.0565	6	1312	115	1349.406	17.297	6.050	9.292	P1	
J042255.90+290701.5	2.054940	1.80	0.0680	6	1312	138	2083.12	6.685	29.186	8.669	P2	E
J042518.63+305018.1	1.265071	1.78	0.1036	8	1312	83	6393.781	9.069	11.243	10.328	P1	E
J045349.66+333842.5	1.843365	4.27	0.0340	6	913	94	422.898	1.694	11.032	8.736	P2	A
J045441.00+335323.2	1.435404	1.97	0.1118	5	913	45	871.943	10.557	2.699	11.698	P1	
J044803.38+342415.5	1.385160	3.10	0.1202	7	913	102	1718.045	15.560	4.113	10.556	P1	
J050328.03+394509.4	1.727674	2.16	0.0431	3	619	61	796.254	7.185	15.228	5.132	P2	R
J050712.55+335934.4	1.389950	2.09	0.0195	6	826	72	351.477	7.992	1.392	8.023	P1	
J050917.50+300309.8	1.923790	1.78	0.0274	5	826	114	373.920	2.815	7.905	6.973	P2	R
J051221.34+300634.9	1.237851	1.87	0.0304	5	822	49	977.310	15.529	0.125	9.080	P1	
J051414.50+350639.9	1.659918	2.47	0.1866	8	816	122	2770.867	14.260	12.015	9.692	P1	E
J051632.17+304921.5	2.558843	5.83	0.0537	8	824	102	404.012	14.722	4.356	9.510	P1	
J052123.50+343759.3	1.911629	2.14	0.1091	6	826	32	822.981	8.824	3.169	12.427	P2	
J052155.26+334037.0	1.820449	2.35	0.0255	3	825	43	274.351	17.576	0.377	7.871	P2	R
J052155.29+311153.2	2.552743	2.33	0.0172	4	823	46	112.207	8.394	0.599	10.579	P2	
J052639.24+341813.9	1.172678	2.78	0.0843	6	826	74	4831.498	60.055	17.855	9.546	P2	E
J053442.52+312922.3	1.675041	2.40	0.0857	3	826	38	2048.602	24.867	0.544	9.203	P1	
J050210.19+222523.8	1.968182	2.78	0.0968	4	834	38	1338.312	7.930	5.896	12.496	P2	
J050241.49+235554.6	4.148943	5.26	0.0753	3	834	40	755.581	6.135	1.365	9.933	P1	
J050642.37+214850.2	1.620502	2.54	0.0857	3	834	35	1264.624	33.940	3.185	9.215	P2	
J051108.55+230632.3	1.709274	2.59	0.0235	4	819	66	948.96	2.809	22.846	7.396	P2	E
J051109.87+222428.3	1.391621	2.90	0.0306	5	834	68	310.172	3.820	3.518	8.258	P2	
J051849.56+211513.6	1.348566	2.28	0.0579	6	834	57	211.862	4.363	1.103	13.136	P2	
J053026.87+350839.4	1.225148	2.16	0.0668	5	524	50	512.587	20.940	5.471	7.767	P1	R
J053428.54+331646.7	1.227779	4.99	0.0672	6	523	86	1357.361	19.554	0.455	7.339	P2	R
J053430.23+331610.6	1.229169	4.73	0.0393	7	523	84	759.293	8.590	0.170	7.700	P1	R
J054511.65+323330.7	1.553595	1.49	0.0486	3	519	20	507.882	9.426	1.155	11.655	P1	
J054645.34+292753.7	1.175271	2.11	0.0620	3	512	31	414.517	1.839	3.775	13.211	P2	A
J055303.05+275339.4	2.410921	3.34	0.0628	3	524	37	1552.535	15.285	4.518	6.238	P1	R
J055557.92+283738.4	1.241766	2.66	0.0198	5	521	51	105.570	1.543	1.690	8.076	P2	A

Tycho-2 and USNO surveys allow the suitability of the remaining candidates to be assessed on the basis of their colours and proximity to potential photometric crowding objects. A custom-built online query-tool was implemented by the Consortium to query a variety of astronomical catalogues at the position of the transit-candidates, returning survey images of the target field and multiwavelength information for the target and nearby objects from which the parent-stellar parameters can be estimated. We refer the reader to Wilson et al. (2006) for more detailed information on this process.

*Luminosity Class and Spectral Type:* As pointed out by Gould & Morgan (2003), roughly 90% of the bright stars surveyed by ground-based exoplanet transit-searches, are giants for which a transiting exoplanet would produce well under 1% dips; this predicts a rather high astrophysical false-positive rate (Brown 2003). Stellar populations in the galactic disk show coherent, restricted velocity distributions (e.g. Binney & Merrifield 1998). The reduced proper motion (hereafter RPM) can be used to kinematically segregate members of nearby stellar populations; in particular its correlation with absolute magnitude allows WASP targets with proper motions (available from the USNO catalogue for most objects) to be roughly classified by Luminosity class. The position of the target in  $\{RPM, (V - K_S)\}$  space is determined using the Tycho-2 V-magnitude (using the observed SuperWASP V-magnitude  $V_{SW}$  as a check), catalogue  $K_S$  and proper motion estimates from the USNO catalogue. The luminosity class division is based upon spectroscopic surveys of a number of nearby objects, in particular the Cayrel et al (2001) catalogue and the Valenti & Fischer (2005) catalogue from the N2K survey, with the luminosity class estimated with reference to this fit (Figure 1). Unknown reddening is in principle a systematic bias with this measure, as it causes the observed  $(V - K_S)$  and RPM to both be artificially higher than the intrinsic properties.

The reduced proper motion diagnostic was checked manually for cases in which it was in any way ambiguous; in particular, the  $\{RPM, (V - K_S)\}$  diagnostic becomes somewhat inconclusive for objects with  $both\ 1.5 \lesssim (V - K_S) \lesssim 2.2$  and  $RPM \lesssim 2$  (Figure 1). Estimates of the astrometric accuracy of stellar positions on the plates used, combined with transformation errors, produce a quality flag in USNO that gives a probability estimate of the reported proper-motion being correct (Monet et al 2003). Low values of this quality flag suggest poor proper motion measurement. We also use the flux-angular diameter relation from interferometric studies (Kervella et al. 2004, Foché & Gieren 1997); given catalogue  $B, K_S$  magnitudes the angular diameter can be inferred and converted into stellar radius using the Hipparcos parallax (if available) to infer distance. If the available information is ambiguous as to the luminosity class of a target, it is reduced in priority.

*Stellar Radius:* For main-sequence stars the transit depth combined with the 2MASS  $(J-H)$  colour also provides an estimate for the spectral type and radius of the parent star, and thus the radius of the putative planet (Ammons et al. 2006). Note that because Ammons et al. (2006) also used 2MASS photometry, transformation from 2MASS into e.g. the Bessell & Brett (1988) system is not required to estimate radii, removing a potential source of systematic error. For dwarfs the  $(J-H)$ -radius relationship suffers from a de-

generacy, in that the relationship turns over at spectral type  $\sim M0$  (Bessell & Brett 1988). As a cross-check, we use  $(V - K_S)$  and  $(B-V)$  to estimate effective temperature (Blackwell & Lynas-Gray 1994; Zombeck 1992), and the radius from the standard temperature-radius relation for main-sequence stars (Gray 1992).  $B$ -magnitudes for this step are taken from USNO,  $V$  from Tycho 2 or if unavailable, from SW-N. The observed transit-depth is used to estimate the planetary radius assuming the occultation is due to the full disk of the planet at maximum depth.  $(V - K_S)$  colors also provide a way to break the  $(J-H)$ -radius degeneracy; should an object show observed  $(V - K_S)$  too blue for a M0 dwarf, the  $(J-H)$  color must correspond to spectral type earlier than M0 - in practice this applies for all the candidates presented here.

SW-N routinely achieves photometric precision  $\sim 5\text{mmag}$  at  $V = 8.5$ , rising to 0.02 mag at  $V = 13$ ; Tycho-2 shows photometric error  $\sim 0.05$  mag at  $V=10.0-11.0$ , rising to 0.11 mag at  $V=11.0-12.0$  (Høg et al. 2000). 2MASS observations of calibration standards show rms residuals of order  $\gtrsim 0.05$  mag in the  $(10 \leq H \leq 14)$  range (Nikolaev et al. 2000, Carpenter 2001), so we may expect photometric errors to be comparable to reddening effects for comparatively high reddening. For example, with absolute magnitude  $M_V \sim 4$ , a typical late-F / early G-dwarf located roughly 200pc from the Sun would be measured at Tycho-2  $V \sim 10.5$  mag. For the fields of interest here, the local HI column density out to this distance is of order  $10^{20} \text{ cm}^{-2}$  (Fruscione et al. 1994), leading to reddening  $E(B-V) \sim 0.02$  and extinction  $A_V \sim 0.06$  (c.f. Binney & Merrifield 1998). Thus a subset of objects in the survey will show uncertain extinction in  $V$  that is comparable to the photometric uncertainty associated with  $(V - K_S)$ . We thus use parameters inferred from the 2MASS  $(J-H)$  color preferentially over  $(V - K_S)$  when the two measures disagree.

The most inflated planet currently known has radius  $R \sim 1.44R_J$  (Charbonneau et al. 2007a), so we regard SW-N candidates with inferred radii  $\lesssim 1.5R_J$  as sensible candidates. However we do not reject outright candidates with slightly larger inferred radii to allow for photometric uncertainty in this detection survey.

Finally we compute, but do not use as a selection criterion, the ratio of observed transit width to that predicted given best-fit stellar parameters,  $\eta = W_{obs}/W$ . In principle we expect genuine exoplanet transits to show  $\eta \sim 1$ , with some range in values due to observational scatter and inclination variations. This figure of merit was introduced and computed for the OGLE transit candidates by Tingley & Sackett (2005); in practice all genuine OGLE transiting planets show  $0.5 \lesssim \eta \lesssim 1$ .

*Positional Matching:* We also visually check the positions localised by the SW-N pipeline against catalogue position for the target used by the automated query tool; in a few cases the measured position was displaced by a small amount from the catalogue position (even subpixel offsets can amount to nearly  $15''$ ; Section 2.1). Even assuming perfect distortion-correction in the pipeline and no error introduced in the conversion of positions between epochs in the catalogues, objects with high proper-motion may have drifted appreciably in the 2-3 decades since some of the catalogue observations were made. In cases where an object is detected at a slightly different location to its catalogue po-

**Table 3.** Lightcurve timing information for the candidates. HJD of mid-transit = 2450000.0 + Epoch.  $\eta$  is the Tingley & Sackett figure of merit for identification with a transiting exoplanet (Tingley & Sackett 2005). Errors here and throughout this report are formal  $1\sigma$  errors on transit model fits to the data.

SWASP ID	Epoch (d)	Period (d)	Duration (h)	Depth (%)	$\eta$	$N_{trans}$	$V_{SW}$
1SWASP J051221.34+300634.9	3218.6880 $\pm$ 0.0009	1.2379 $\pm$ 2.7 $\times 10^{-5}$	1.872 $\pm$ 0.048	3.04 $\pm$ 0.09	0.77	5	10.90
1SWASP J031103.19+211141.4	3193.2342 $\pm$ 0.0023	2.7301 $\pm$ 1.03 $\times 10^{-4}$	3.46 $\pm$ 0.12	4.03 $\pm$ 0.14	0.94	5	12.23
1SWASP J032739.88+305511.3	3194.3954 $\pm$ 0.0014	1.0512 $\pm$ 2.60 $\times 10^{-5}$	3.00 $\pm$ 0.07	2.53 $\pm$ 0.08	1.06	14	12.17
1SWASP J051849.56+211513.6	3219.3183 $\pm$ 0.0024	1.3486 $\pm$ 6.20 $\times 10^{-5}$	2.28 $\pm$ 0.12	5.79 $\pm$ 0.39	0.88	6	12.05

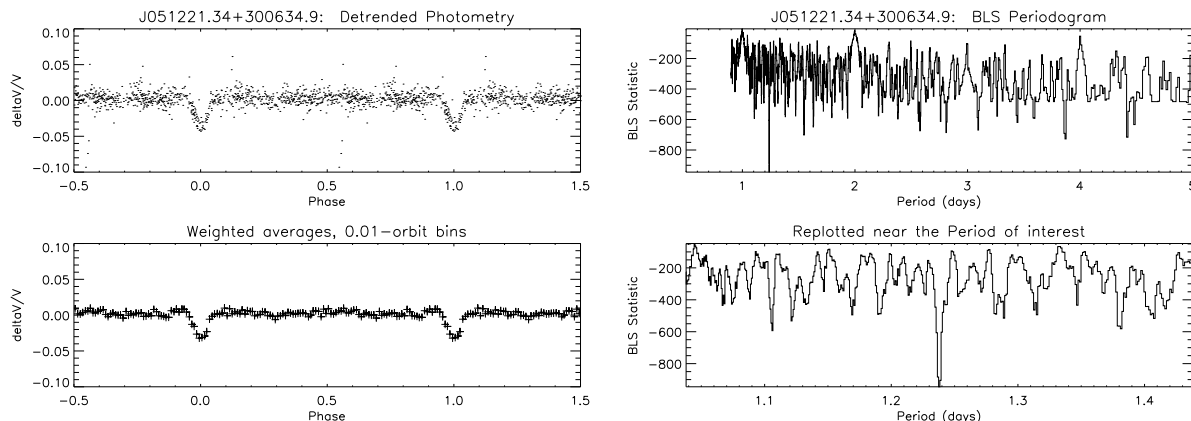


**Figure 2.** The accepted Priority 1 Candidate J051221.34+300634.9. *Left:* Folded lightcurve. Top panel: folded lightcurve after detrending. Bottom panel: phase-binned averages weighted by  $(1/\sigma_i^2)$ , where  $\sigma_i^2$  is the estimated variance on each datapoint including both formal and systematic error (section 3.1). *Right:* Box Least Squares periodogram.

sition, the automated catalogue query tool can misidentify the target as a blending neighbour. In these cases we use the measured magnitude  $V_{SW}$  to determine the most likely matching catalogue object, and re-calculate the diagnostics accordingly.

*Crowding:* Candidates were rejected outright if any object brighter than the candidate was present within the 48'' SW-N aperture. For candidates with nearby objects *fainter* than the candidate, we calculate the magnitude of the nearby object that would be required for a 50%-depth eclipse from the object to produce the observed transit-depth from the aperture; if this magnitude is surpassed the candidate is rejected.

## 4 RESULTS

The bottom line of this analysis is that one out of 2688 candidates is put forward as a Priority 1 target for spectroscopic follow-up with three of 2688 Priority 2 targets. Table 1 gives the field statistics for the search. Table 2 lists the 44 objects surviving visual inspection, Table 3 gives the four candidates finally accepted. We provide notes on the accepted objects below, as well as a subset of the rejected candidates. Some of the rejected objects are of interest in their own right, either because their rejection is illustrative of the procedures we followed to filter out candidates, or because the objects are astrophysically interesting (Section 4.3).

### 4.1 Priority 1 Candidate

Only one object assigned Priority 1 on the basis of the visual and S/N cuts (Section 3.2) survived the application of catalogue information. See Figure 2 for its lightcurve and BLS periodogram.

**1SWASP J051221.34+300634.9:** This object shows an almost prototypical transit-candidate event of 3%-depth over a flat out-of-transit lightcurve. Five transits are observed with a 1.24-day period and 1.87-hour transit duration. With reduced proper motion 2.19 and  $(V-K_S)=1.61$ , this object is firmly in the dwarf regime (Figure 2). Two USNO objects are  $\gtrsim 4.37$  magnitudes fainter than the target within the 48'' SW-N aperture, and thus are too faint to produce blending at the detected transit level. 2MASS  $(J-H)=0.26$  suggests a 1.15  $R_\odot$  F9 primary, implying planet radius 1.71  $R_J$  and Tingley & Sackett  $\eta=0.77$ .

### 4.2 Priority 2 Candidates

Two objects were initially assigned Priority 1 from visual analysis and the S/N cuts in Section 3.2; however inclusion of prior information from catalogues highlighted some uncertainty in the luminosity class of these objects, thus they were demoted to Priority 2. One further object that was initially assigned Priority 2, survived the inclusion of catalogued information. Periodograms and lightcurves for all three objects can be found in Figure 3.

**1SWASP J031103.19+211141.4:** Deep (4.03%), clearly visible transit events are present, though there may



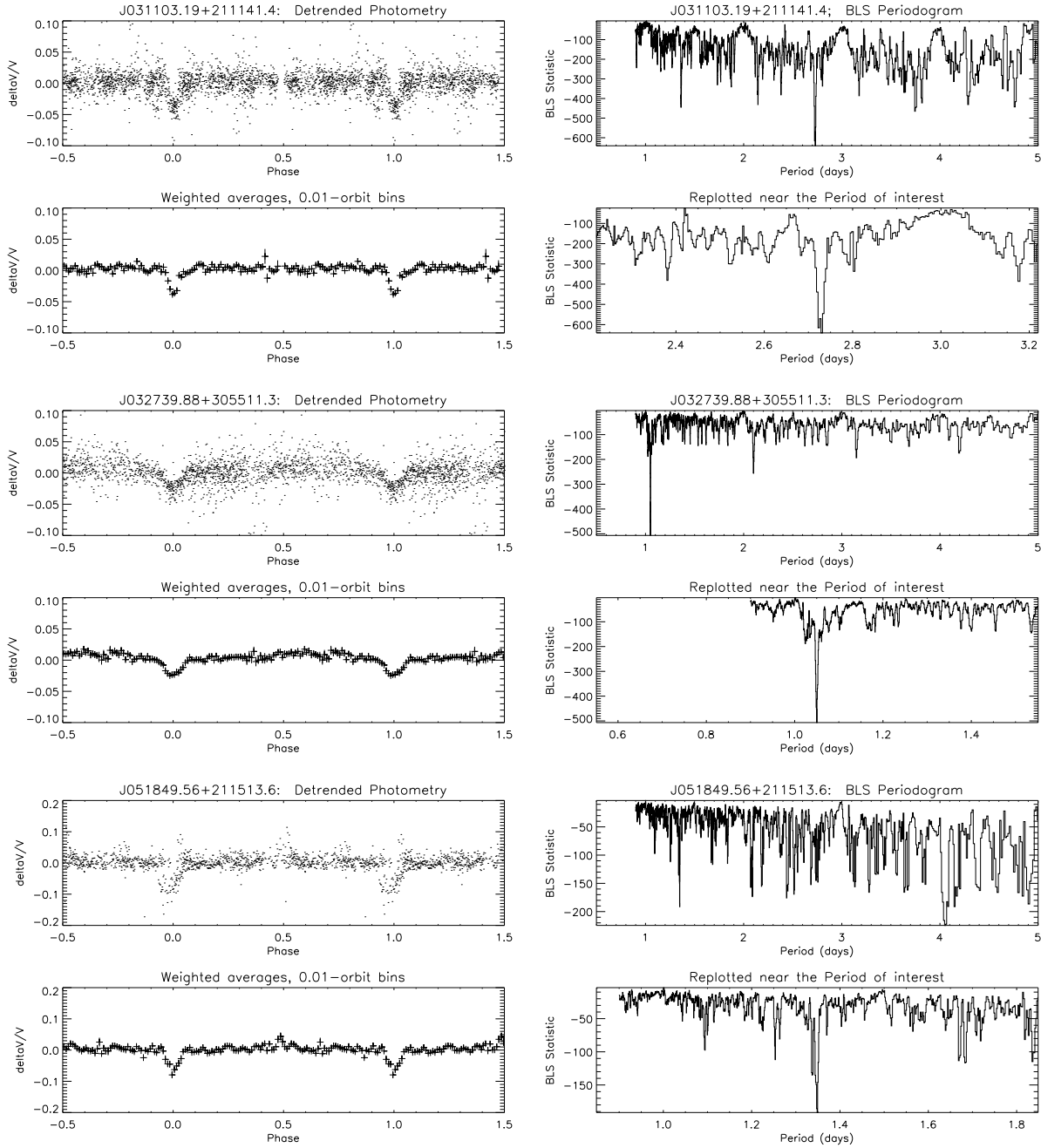


**Figure 3.** The accepted Priority 2 Candidates: Folded lightcurves and BLS periodograms for (from top to bottom): J031103.19+211141.4; J032739.88+305511.3; J051849.56+211513.6.

be some structure in the transit besides a planetary-type event. No Tycho-2 or *Hipparcos* objects are found at the object position or within a  $48''$  radius, making stellar radius determination using the apparent diameter relations of Kervella et al (2004) impossible. USNO lists no potential blends within the SW-N aperture. The luminosity class of this object is somewhat open to question. USNO reports a bad measurement for proper-motion, so the reduced proper motion has nothing to say about the luminosity class of this object (at  $V-K_S=1.88$  this measure would be ambiguous for this object for proper-motions  $\lesssim 8\text{mas yr}^{-1}$ ).

Assuming the parent star is luminosity-class V, 2MASS  $(J-H)=0.27$  implies parent spectral type G0 and radius  $\sim 1.12 R_\odot$ . This implies a planetary radius  $\sim 1.89 R_J$ , with Tingley & Sackett figure of merit  $\eta=0.94$ , just within the range corresponding to likely exoplanet transits (Tingley & Sackett 2005).

**1SWASP J032739.88+305511.3:** This object shows a clear shallow transit-like event (2.53%), on a 1.05 day period clearly distinct from the 1-day trough in the periodogram (Figure 3); at this period, fourteen transits are observed. No *Hipparcos* or Tycho-2 objects are found at the

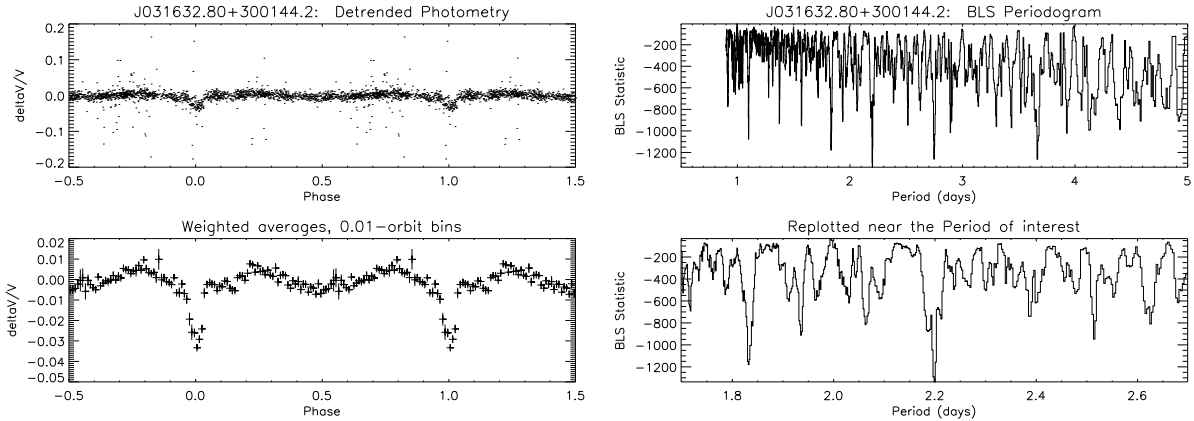


**Figure 4.** Phase-folded lightcurve and BLS periodogram of the otherwise excellent transit candidate 1SWASP J031632.80+300144.2. *Left:* the phase-folded lightcurve as it would appear at the visual examination stage (top) and re-plotted on a compressed flux-scale (bottom); the existence of ellipsoidal variations is clear. (Compare with Figure 1 of Sirko & Paczyński 2003.) *Right:* the BLS periodogram.

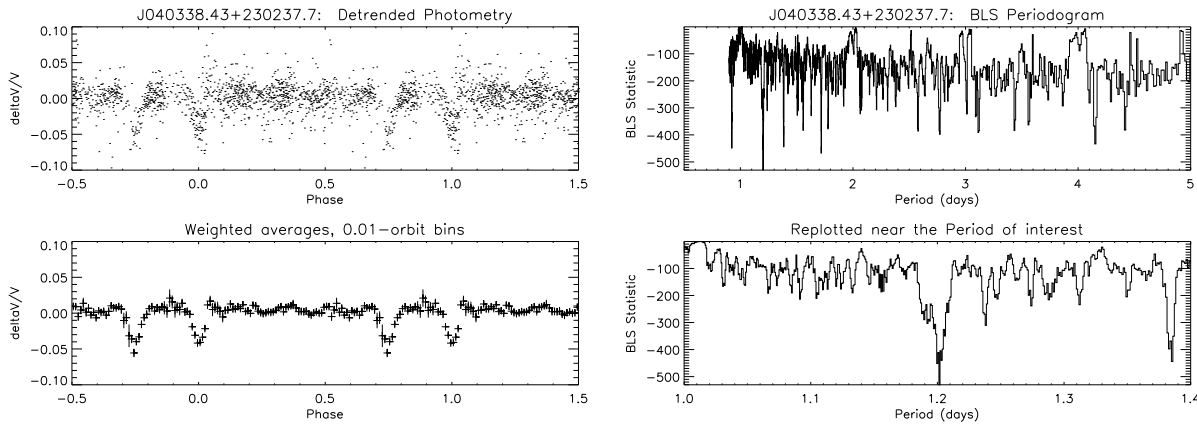


**Figure 5.** Folded lightcurve and periodogram for the possible eccentric-orbit system J040338.43+230237.7.

target position or within  $48''$  of the target, so direct inference of the stellar radius (c.f. Kervella et al. 2004) is not possible. USNO lists no potential blending objects within the SW-N aperture. As with J031103.19+211141.4, the USNO proper motion measurement cannot be used due to poor quality (Section 3.3). However, with  $(V-K_S) \sim 2.9$ , this object would have to show proper-motion  $\gtrsim 15 \text{ mas yr}^{-1}$  to be close enough to be a likely dwarf (Figure 1), which is rather high to go unnoticed over the 25-year timebase of the USNO catalogue. Thus there is the suspicion that this object may be a giant and it was thus demoted to Priority 2. Color index 2MASS  $(J-H) = 0.22$  suggests a  $1.23 R_\odot$  parent with spectral type F8, *assuming* it falls on the main-sequence. This predicts planet radius  $1.69 R_J$  and Tingley & Sackett  $\eta = 1.06$ .

**1SWASP J051849.56+211513.6:** This object shows six transit-like events of  $\sim 6\%$  depth on a 1.35-day period and with a 2.3-hour transit duration. The transit lightcurve is rather deep and possibly V-shaped, however consistent with a planetary transit given the photometric precision (Figure 3). With reduced proper motion  $\sim 1.62$  and  $(V-K_S) = 2.2$ , this object lies within a region of parameter space roughly equally populated by dwarfs and giants, thus its luminosity class is uncertain. *Assuming* the par-

ent star is a main-sequence object, the 2MASS colors  $(J-H) = 0.27$  suggest a  $1.12 R_\odot$  G0 primary, implying planetary radius  $2.3 R_J$  and Tingley & Sackett  $\eta = 0.88$ , so these parameters are consistent with a transiting exoplanet. In addition to the luminosity-class uncertainty for this object, the lightcurve shows possible variability at anti-transit, and when folded on the most significant BLS period-detection (4.05 days) only shows two transits (we used the next most-significant period of 1.35 days in this analysis). This object is thus kept at Priority 2 pending further lightcurve sampling in the upcoming 2006 dataset.

### 4.3 Example Rejected Candidates

**1SWASP J031632.80+300144.2 - ellipsoidal variations:** This object shows six transit-like events of  $\sim 3.1\%$  depth; at this signal-to-noise the folded profile (Figure 4) is not entirely symmetric in the region of the transit, though this may still be an artefact of the reduction. The 2.199-day period is clearly distinct from any aliases in the periodogram, and photometric colours imply late-G/early-K-type main-sequence parent star. However, the signal-to-noise of ellipsoidal variations is high, at  $\sim 26$ , and indeed a replotting of the lightcurve on a wider phase-scale and com-

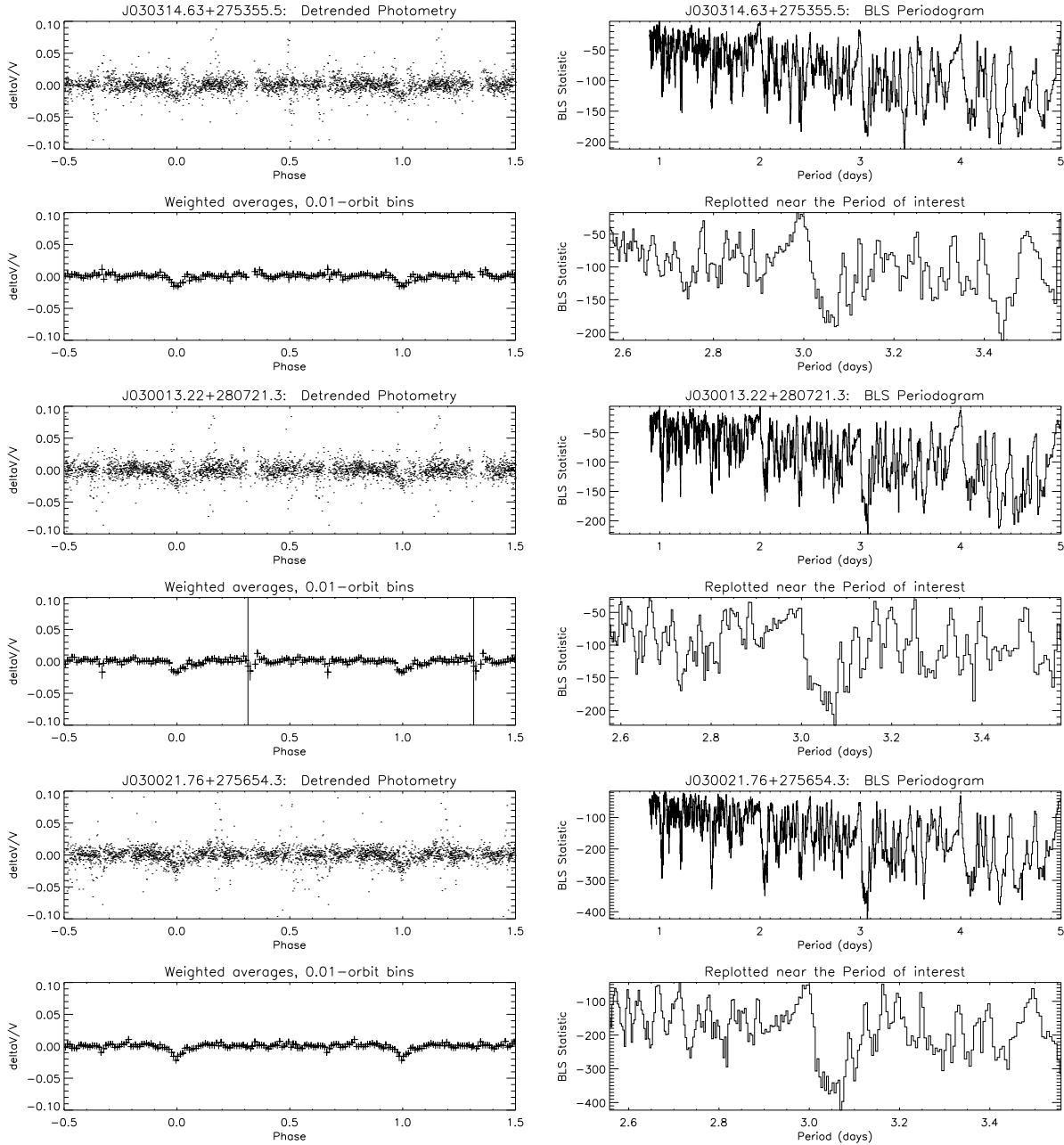


**Figure 6.** Folded lightcurves and periodograms (after detrending) for the objects J030314.63+275355.5 (top), J030013.22+280721.3 (middle) and J030021.76+275654.3 (bottom). Detected periods are 3.07125, 3.070201 and 3.0577 days respectively (from top to bottom). The nearest pair are 10.7 arcmin (43 pixels) from each other but show such similar folded lightcurves and periods that we reject all three as possible candidates.

pressed flux-scale shows quite clearly the existence of apparently ellipsoidal variations (compare with e.g. Figure 1 of Sirko & Paczyński 2003). This object is probably a grazing-incidence stellar binary.

**J040338.43+230237.7 - eccentric-orbit binary?**

This object shows pairs of occultations at different depths when folded on the detected period of  $1.20 \pm (4.1 \times 10^{-5})$  days, but for which the secondary events are far from phase 0.5 (Figure 5). The transit-like events are well-sampled, with seven transit-like events observed. Further analysis of this interesting object will be reported in a future paper.

**J044639.17+394837.6 - blend:** This object is apparently very heavily blended and its catalogue magnitudes (e.g.  $B \sim 16.5$ ; no Tycho-2  $V$ -magnitude is present for this object) are far from those measured ( $V_{sw} \sim 12.0$ ). The nearby ( $22''$ ) object USNO 1298-0108374 has Tycho-2  $V$  magnitude  $V_{Ty2} \sim 12.3 \pm 0.4$ , much closer to  $V_{sw}$ . It is surrounded by 8 objects within 3.5-5 magnitudes, however, which could contribute up to  $\sim 20\%$  of the light in the aperture. Thus both candidate counterparts are too blended to allow a planetary companion for the observed depth of eclipse-like event.

**J045349.66+333842.5 - X-ray faint H $\alpha$  emission-line object:** Rejected because two blended objects are within 5 magnitudes, *Simbad* shows this to be an H $\alpha$  emission-line object. No *ROSAT* source is detected. With a 1.8d period, this might be an X-ray faint active binary with low-amplitude optical variability.

**J040322.73+274841.5 - spectral type uncertainty, blend:** With transit depth 2%, this object exhibits 4 transits in the SW-N 2004 dataset against otherwise smooth behaviour outside “transit.” In addition to the candidate, two red objects are found within the aperture that are only two magnitudes fainter in  $JHK_S$  and with USNO magnitude difference from the candidate  $\Delta R \sim 5.2$ ,  $\Delta I \sim 3.5$ . There is a third neighbour  $< 10''$  distant, but it is roughly  $\sim 7$  mags fainter (by comparison with a well-separated nearby object of similar apparent brightness in the DSS image). While  $(B - V) \sim 0.3$  suggests spectral type roughly  $\sim F0$  or so (Zombeck 1992), the  $(V_{sw} - K)$  and  $(J - H)_{2MASS}$  suggest spectral type closer to late-F or early-G. As the SW-N bandpass includes Johnson  $RI$ , (c.f. Figure 2 of Kane et al 2004), this object may well be blended at the 1% level in the SW-N bandpass.

**J030021.76+275654.3 - artefact:** This object was originally a Priority 2 transit candidate. However its period and periodogram are highly similar to a number of other distinct stellar objects in the image. The zeropoints in the fitted ephemerides for each object are highly similar - with an  $MJD_0$  spread of only 1.5 hours - suggesting the apparent period detection may have been dominated by lightcurve artefacts still present after detrending (Figure 6). The detrending and BLS period-search (section 3.2) produces a few hundred exoplanet-candidates per field, which allows a simple check for candidates that share the same period as several other objects, such as J030021.71+27654.3. In principle the lightcurves of all candidates might be examined with reference to the raw image, to determine if such groups of candidates cluster near any bright, variable object or along artefacts such as CCD bleeds. This requires a detailed, highly accurate knowledge of the wings of the PSF both as a function of on-chip position, and of frame-number. A simple plot of the position of the candidates with similar periods shows that in fact these objects are *not* near any extremely bright object; Figure 7.

A more efficient if cruder method is to search for peaks in the distribution of detected periods to catch groups of highly similar detected periods. The distribution of detected periods is highly field-dependent (Figure 8), so we cannot sum over fields to improve the statistics for this process. We see that for the field containing J030021.76+275654.3 (field SW0316+3126) there is indeed a rather high number (ten) of objects with detected period  $3.06 \pm 0.015$  days. This highlights a number of other suspicious periods from the fields observed. Candidates at these periods were *not* rejected outright based on the period alone, but their lightcurves and periodograms were compared to other objects with similar detected period to screen for possible artefacts. The sample in Figure 8 contains lightcurves both with and without significant sampling gaps - these are the lightcurves for all objects passed forward for visual selection by the initial BLS period-search and statistical cuts (Section 3.2). Objects where the automated search has fit sampling-gaps or any residual nightly trends, cluster at 1-day periods; these ob-

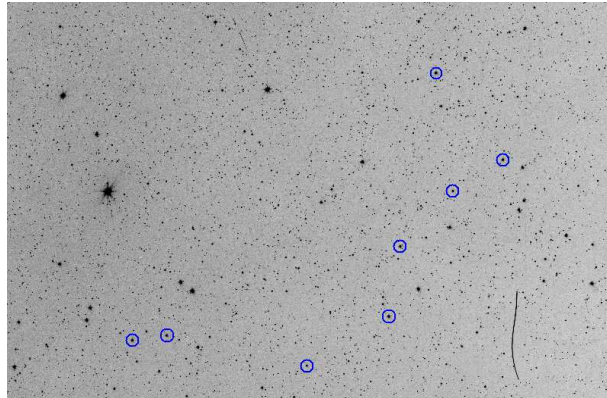


**Figure 7.** The spatial distribution of objects in field SW3016+3126 with periods  $3.06 \pm 0.015$  days (of which three example lightcurves are plotted in Figure 6), overlaid on a Digitized Sky Survey image (North to top, East to left; the figure measures  $90' \times 60'$  and the objects are marked with circles). No obvious pattern (such as proximity to a bright source) is seen in the spatial distribution of artefacts. (One further object  $\sim 60'$  to the East of this image is not shown).

jects are not considered further. The general shape of the distribution of detected periods does appear to broadly follow the number of nights in each field, though the distribution of periods detected clearly does not depend just on the number of nights alone (Figure 8). For example, fields SW0344+2427 and SW0543+3126 show similar drops to zero detections at or near periods of integer days, and both are the most sparsely-sampled fields in this RA range (Table 1).

**J032113.37+301909.5 & J032112.56+301910.9 - visual double:** Two separate objects are reported by the WASP pipeline with similar lightcurves and periodograms, and positions  $\sim 12''$  apart. The closeness on-sky of the two lightcurves threw immediate suspicion on either of these objects as planet-host candidates, which was confirmed at the stage of catalogue examination. Four catalogues of visual doubles provide matches with this object; the Cousteau catalogue of 2700 doubles (Cousteau 1995), the Washington Visual Double Star catalogue (Worley & Douglas 1997), the CCDM (Dommanget et al. 2002) and the Tycho Double Star Catalogue (Fabricius et al. 2002); this object is the visual double CCDM J03212+3019A & B. The primary is listed as spectral type A5 (luminosity class not determined), and objects A & B have V-magnitudes 10.4 and 12.5 respectively. The recurrence interval for the transit-like events is 2.26742(5) days, which is rather short for a fully detached binary; however the significance of any ellipsoidal variation is low (at S/N of ellipsoidal variations  $\lesssim 1.7$ ; see also the lightcurve in Figure 9). One possible scenario is that the fainter object B may be deeply eclipsed by a third, unseen object. Although only  $\sim 2/3$  SW-N pixels apart, the two components do produce an extended object under a  $15''$  pixel-scale (Figure 9); initial source-finding with *SExtractor* (Bertin & Arnouts 1996) localised this to two separate peaks which were each reduced with the WASP pipeline. Although clearly a blend, this object did not fall within the locus of blended objects based on comparison of flux within the three SW-N apertures, because the object extension falls almost

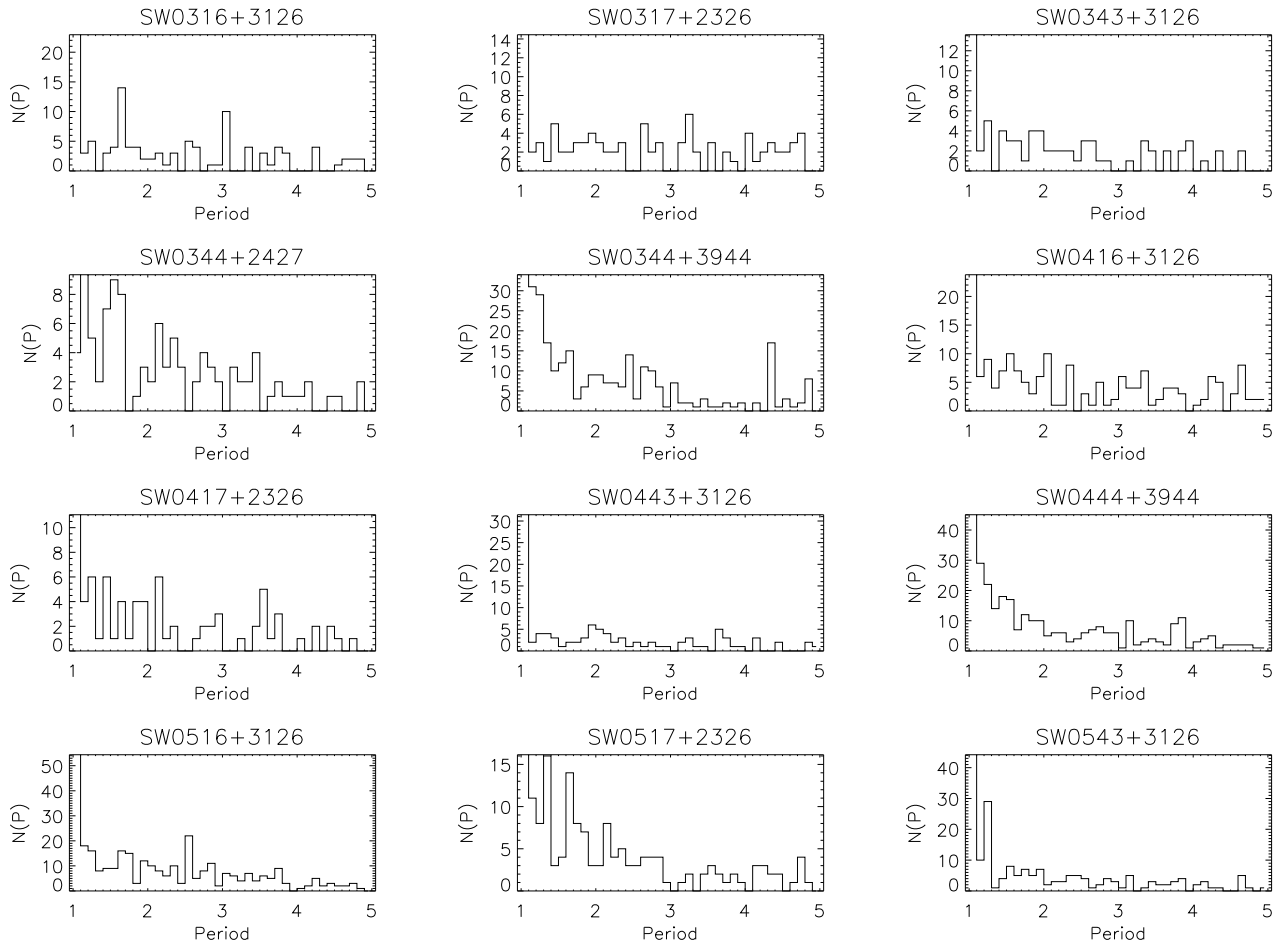


**Figure 8.** Periodicities returned from BLS period-search on lightcurves that have been detrended (Tamuz et al. 2005). Local increases in detected period represent possible shared-variability artefacts such as J030021.76+275654.3. The periods at which these likely artefacts occur are highly field-dependent. For example, the field SW0316+3126 (top left) shows ten objects with periods  $3.06 \pm 0.015$  days. Examination of the lightcurves and periodograms of these objects shows a population of objects with shared variability, which must be removed from further consideration (Figure 6).

entirely within the innermost aperture (Figure 9). Further examination of this object will be reported elsewhere.

## 5 DISCUSSION

Of a total of 141,895 targets extracted for the transit-search in the fields considered here, 2688 were selected as potential photometric transit candidates at the initial selection by  $S_{red}$  and cadence by the BLS algorithm (Collier Cameron et al. 2006). Of these, 44 passed the visual tests. The subsequent statistical tests removed all but 20 of the candidates, of which 4 passed tests imposed by existing catalogue photometry at higher spatial resolution; this last stage led to the demotion of two otherwise Priority 1 objects. One object was passed forward as a Priority 1 candidate for follow-up with other facilities, with three more flagged as Priority 2 possibilities. As the other WASP candidate-lists produced thus far (Christian et al. 2006, Lister et al. 2007, Street et al. 2007) have resulted in  $\sim 3$ -4 times as many good candidates as the fields we report here, it is worth examining the expected planet yield for the 03–06h RA range.

The relative dearth of transit candidates reported here is almost certainly a result of the comparatively sparse sampling for this RA range; the most intensively-observed field here consisted of 1885 frames over 60 nights, compared to e.g. 5541 frames over 127 nights for a field on the other side of the sky (c.f. Street et al. 2007). This has two key effects on our ability to detect transits. The first effect was predicted before the survey began: even with purely uncorrelated noise and an ideal instrument, the rotation of the Earth imposes period-ranges in regions about integer-day periods, within which the likelihood of detecting transits is reduced. As the Earth orbits the Sun and the sky precesses throughout the year, the width of these intervals is reduced. These low-observability windows are superimposed on a general decrease in probability of transit observability with period due to fewer numbers of long-period cycles falling within a typical observing season. To clarify this point we present example estimates of the probability of observing  $N$  or more transits in a single SW-N observing season, computed for each field as a byproduct of the transit search (Collier Cameron et al. 2006), with the true sampling of each field as an input (Figure 10). As can be seen, below about

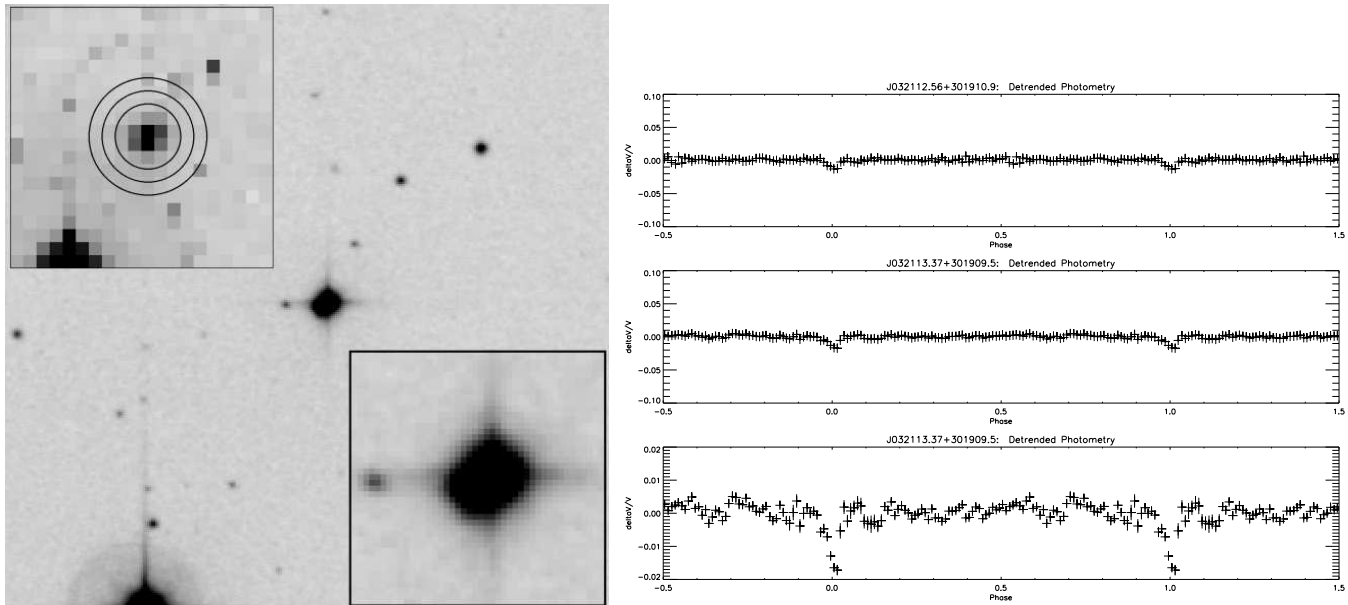


**Figure 9.** The visual double CCDM J031212+3019A & B, recorded by the WASP pipeline as 1SWASP J032113.37+301909.5 & J032112.56+301910.9 (Section 4.3). *Left:* Digitised Sky Survey image of the  $5' \times 5'$  region surrounding the two objects, with the immediate region surrounding the target (inset lower-right: the inner  $30'' \times 30''$ ) and the full region binned to  $15'' \times 15''$  pixels, approximately matching the SW-N pixel scale; Section 2.1 (inset upper-left). North is up, East to the left. The three SW-N apertures used for blending tests (2.5, 3.5 & 4.5 pixels) are denoted by concentric circles. At  $\sim 12''$  separation, the two components of the visual binary are so close that the resulting source extension under SW-N pixellation in the binned image falls entirely within the innermost aperture; thus the curve-of-growth blending index based on the three SW-N apertures misses the resulting blend. *Right:* Lightcurves of the two objects found by *SExtractor* during the pipeline reduction. At 2.27 days the recurrence interval is rather short for a fully detached stellar binary; however, little indication is found for ellipsoidal variations (bottom right).

60 nights' data-length, the recoverability of transits drops dramatically for all but the shortest periods.

The second key effect of short observing timescales is the loss of sensitivity in the presence of strong variability from correlated noise, in which the noise power is not independent of the timescale of variability. When planning ground-based transit searches, it was largely assumed that improved reduction techniques would result in uncorrelated noise (e.g. Horne 2003). In practice, despite the fact that the magnitude of noise variation from several transit-surveys (ours included) approach the Poisson floor for the entire magnitude range over which we are sensitive to transits (here  $8 \lesssim V \lesssim 13$ ), correlated noise continues to be a significant source of potential false-positives, with significant power to variations with  $\sim 2.5$ h duration (similar to a genuine exoplanet transit). The only ground-based broad-shallow transit-search team we are currently aware of that claims uncorrelated noise is the XO group, which employs drift-scanning to smooth out systematic trends instrumentally (McCullough et al. 2006); thus it appears that correlated noise of this nature may be a feature of the observational strategy we have chosen. The full signal to noise statistic  $S_{red}$  of Pont et al. (2006) provides a measure of the signal to noise of a transit detection in the presence of correlated noise, and thus provides a useful measurement to investigate ways to tame frequency-dependent correlated noise. In particular we note the following two key results from the considerations of Pont et al (2006): (i) that for ground-based transit surveys the threshold to detect transits in the presence of correlated noise is typically a factor

$\sim 3$  higher than in the presence of uncorrelated noise alone, and that (ii) in the presence of correlated noise,  $S_{red}$  should scale roughly linearly with the total number of nights of observation. The latter is particularly important, and can be easily understood in the following way: consider a transit signal with transit-duration  $\delta_t$  and period  $P_t$ . The presence of correlated noise with significant power at timescales  $\sim \delta_t$  will add spurious transit-like events at randomised phases, reducing the coherence of the resulting transit lightcurve and making the true periodicity more difficult to separate out from the noise. Although comparison of the badness-of-fit allowing a model consisting of both positive and negative transit-like events with that from negative transits only (c.f. Burke et al. 2006) can to some extent estimate the impact of correlated noise on the lightcurve itself, it is clear that characterisation of the true transit period in this case really requires as long an observing season as possible.

Indeed, simulations applied specifically to the WASP project (Smith et al. 2006) suggest  $S_{red}$  should increase roughly linearly with the number of nights of observation; Smith et al (2006) suggest that  $\sim 19 \pm 8$  genuine detections should be expected from the entire WASP-N 2004 dataset; at  $\lesssim 60$  nights the recovery fraction drops to roughly a quarter of that expected for datasets of length  $\sim 120$  nights. Our yield of four candidates is consistent with this scaling.

## 6 CONCLUSIONS

One Priority 1 exoplanet transit candidate has been uncovered from the 03–06h RA fields in the WASP-N 2004 dataset

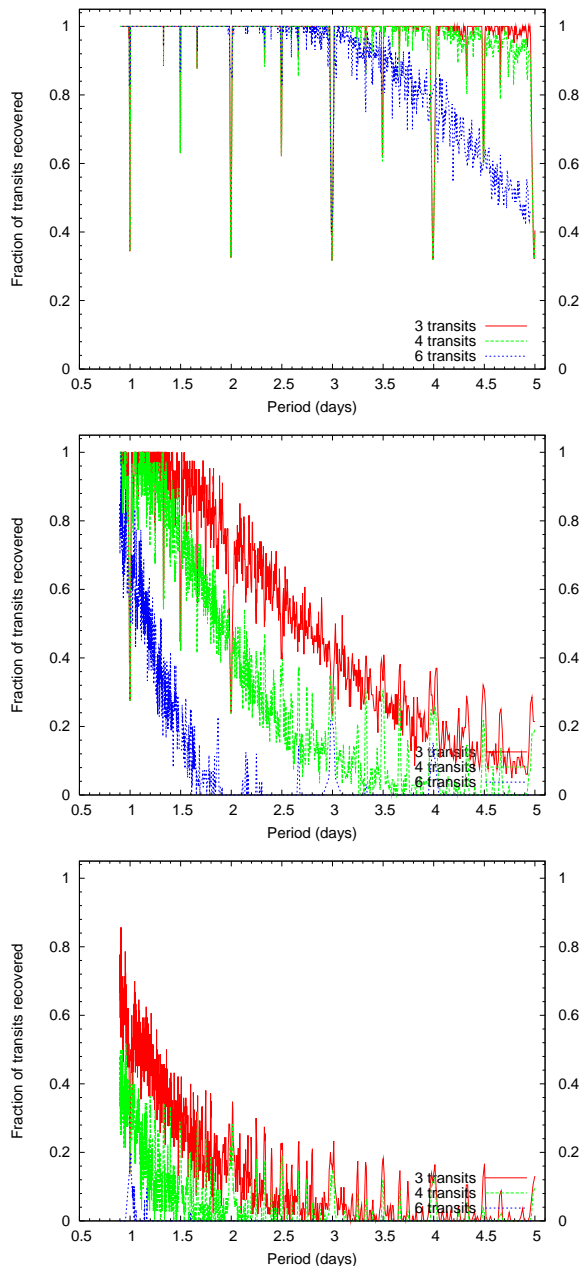


**Figure 10.** Probability of transit detection as a function of planetary orbital period, for three (solid lines), four (dashed lines) and six (dotted lines) transits (see Collier Cameron et al. 2006). The coverage for these fields is as follows: **Top:** 5441 frames over 129 nights (field 2045+1628); **Middle:** 1402 frames over 64 nights (field SW0343+3126), **Bottom:** 544 frames over 37 nights (SW0543+3126). There is a marked gradient in observability of transits with the number of nights observed; for 37 nights of data, the recovery fraction at 4 transits drops to 10 percent at all periods  $\gtrsim 1.5$  days.

and three Priority 2 objects. This number is lower than that produced by other fields with longer observation timebases. This is certainly due to the comparatively sparse sampling, which bears out in a qualitative way the results of recent work on correlated noise in ground-based photometric surveys. When the 2006 SuperWASP datasets are fully reduced,

we expect to find many more candidates for follow-up work as a result of the longer baseline this allows.

## ACKNOWLEDGMENTS

The WASP consortium consists of representatives from the Queen’s University Belfast, University of Cambridge (Wide Field Astronomy Unit), Instituto de Astrofísica de Canarias, Isaac Newton Group of Telescopes (La Palma), University of Keele, University of Leicester, Open University, and the University of St Andrews. The SuperWASP-North and South instruments were constructed and operated with funds made available from Consortium Universities and the Particle Physics and Astronomy Research Council. SuperWASP I is located in the Spanish Roque de Los Muchachos Observatory on La Palma, Canary Islands which is operated by the Instituto de Astrofísica de Canarias (IAC). Several large astronomical catalogues were used via the *VizieR* service, operated at CDS in Strasbourg, France, primarily the Tycho-2 and USNO catalogues. This publication makes use of data products from the Two Micron All Sky Survey, which is a joint project of the University of Massachusetts and the Infrared Processing and Analysis Center/California Institute of Technology, funded by the National Aeronautics and Space Administration and the National Science Foundation. The Digitized Sky Surveys were produced at the Space Telescope Science Institute under U.S. Government grant NAG W-2166. The images of these surveys are based on photographic data obtained using the Oschin Schmidt Telescope on Palomar Mountain and the UK Schmidt Telescope. The plates were processed into the present compressed digital form with the permission of these institutions. We have made use of the Extrasolar Planets Encyclopaedia, maintained on-line by Jean Schneider at <http://exoplanet.eu/catalog.php>.

We thank the anonymous referee for a number of insightful comments that greatly improved this manuscript. WIC thanks Peter McCullough and Kailash Sahu for fruitful discussion.

## REFERENCES

- Aigrain, S. & Favata, F. 2002 *A&A* 395, 625
- Aigrain, S. & Irwin, J. 2004 *MNRAS* 350, 331
- Ammons, S. M., Robinson, S.E., Strader, J., Laughlin, G., Fischer, D., Wolf, A., 2006 *ApJ* 638, 1004
- Bakos, G., Noyes, R. W.; Kovács, G.; Latham, D. W.; Sas-selov, D. D.; Torres, G.; Fischer, D. A.; Stefanik, R. P.; Sato, B.; Johnson, J. A.; Pál, A.; Marcy, G. W.; Butler, R. P.; Esquerdo, G. A.; Stanek, K. Z.; Lázár, J.; Papp, I.; Sári, P.; Sipőcz, B., 2007 *ApJ* 656, 552
- Bertin, E. & Arnouts, S., 1996 *A&AS* 117, 393
- Bessell, M.S. & Brett, J.M. 1988 *PASP* 100, 1134
- Binney, J.J. & Merrifield, M. 1998, *Galactic Astronomy*, 1st edition, Princeton University Press
- Blackwell, D. E. & Lynas-Gray, A. E., 1998, *VizieR On-line Data Catalog: J/A+AS/129/505*, see also *A&AS* 129, 505
- Bouchy, F., Pont, F., Melo, C., Santos, N. C., Mayor, M., Queloz, D., Udry, S. 2005 *A&A* 431, 1105
- Brown, T.M., 2003 *ApJ* 593, L125

- Brown, T.M., Charbonneau, D., Gilliland, R. L., Noyes, R. W., Burrows, A., 2001 ApJ 552, 699
- Burke, C.J., Gaudi, B. S., DePoy, D. L., Pogge, R. W., 2006 AJ 132, 210
- Carter, B.S. 1990 MNRAS 242, 1
- Cayrel de Strobel, G., Soubiran, C., Ralite, N., 2001 A&A 373, 159
- Charbonneau, D., Brown, T. M., Noyes, R.W., Gilliland, R. L., 2002 ApJ 568, 377
- Charbonneau, D. Winn, J.N., Latham, D.W., Bakos, G., Falco, E.E., Holman, M.J., Noyes, R.W., Csák, B., Esquerdo, G.A., Everett, M. E., O'Donovan, F.T., 2006 ApJ 636, 445
- Charbonneau, D., Brown, T.M., Burrows, A., Laughlin, G., 2007a in *Protostars and Planets V*, eds. Reipurth, V.B., Jewitt, D. & Keil, K., University of Arizona Press, p701-716, see also astro-ph/0603376
- Charbonneau, D., Winn, J. N., Everett, M. E., Latham, D. W., Holman, M. J., Esquerdo, G. A., O'Donovan, Francis T., 2007b ApJ in press, astro-ph/0610589
- Christian, D.J., Pollacco, D. L., Skillen, I., Street, R. A., Keenan, F. P., Clarkson, W. I., Collier Cameron, A., Kane, S. R., Lister, T. A., West, R. G., Enoch, B., Evans, A., Fitzsimmons, A., Haswell, C. A., Hellier, C., Hodgkin, S. T., Horne, K., Irwin, J., Norton, A. J., Osborne, J., Ryans, R., Wheatley, P. J., Wilson, D. M., 2006 MNRAS 372, 1117
- Collier Cameron, A., Pollacco, D., Street, R. A., Lister, T. A., West, R. G., Wilson, D. M., Pont, F., Christian, D. J., Clarkson, W. I., Enoch, B., Evans, A., Fitzsimmons, A., Haswell, C. A., Hellier, C., Hodgkin, S. T., Horne, K., Irwin, J., Kane, S. R., Keenan, F. P., Norton, A. J., Parley, N. R., Osborne, J., Ryans, R., Skillen, I., Wheatley, P. J., 2006 MNRAS 373, 799
- Collier Cameron, A., Bouchy, F., Hbrard, G., Maxted, P., Pollacco, D., Pont, F., Skillen, I., Smalley, B., Street, R. A., West, R. G., Wilson, D. M., Aigrain, S., Christian, D. J., Clarkson, W. I., Enoch, B., Evans, A., Fitzsimmons, A., Fleenor, M., Gillon, M., Haswell, C. A., Hebb, L., Hellier, C., Hodgkin, S. T., Horne, K., Irwin, J., Kane, S. R., Keenan, F. P., Loeillet, B., Lister, T. A., Mayor, M., Moutou, C., Norton, A. J., Osborne, J., Parley, N., Queloz, D., Ryans, R., Triaud, A. H. M. J., Udry, S., Wheatley, P. J., 2007 MNRAS 375, 951
- Couteau, P., 1995, *VizieR On-line Data Catalog: I/209A*
- Deming, D., Seager, S., Richardson, L.J., Harrington, J., 2005a Nature 434, 740
- Deming, D., Brown, T.M., Charbonneau, D., Harrington, J., Richardson, L.J., 2005b ApJ 622, 1149
- Dommanget, J. & Nys, O. 2002 *VizieR On-line Data Catalog: I/274*
- Fabricius, C., Høg, E., Makarov, V. V., Mason, B. D., Wycoff, G. L., Urban, S. E., 2002 A&A 384, 180
- Foqué, P. & Gieren, W.P., 1997 A&A 320, 799
- Fruscione, A., Hawkins, I., Jelinsky, P., Wiercigroch, A., 1994 ApJS 94, 127
- Glass, I.S., 1999, *Handbook of Infrared Astronomy*, Cambridge University Press, 1st Edition
- Gould, A., Morgan, C. W., 2003 ApJ 585, 1056
- Gray, D.F. 1992, *The Observation and analysis of stellar photospheres*, 2nd ed., Cambridge University Press
- Høg, E., Fabricius, C., Makarov, V. V., Urban, S., Corbin, T., Wycoff, G., Bastian, U., Schwekendiek, P., Wicenc, A., 2000 A&A 355, 27
- Homer, L., Charles, P. A., Hakala, P., Muhli, P., Shih, I.-C., Smale, A. P., Ramsay, G., 2001 MNRAS 322, 827
- Horne, K. 2003, in ASP Conference Series vol. 294, *Scientific Frontiers in Research on Extrasolar Planets*, eds. D. Deming & S. Seager (San Francisco: ASP), 361
- Kane, S.R., Collier Cameron, A., Horne, K., James, D., Lister, T.A., Pollacco, D.L., Street, R.A., Tsapras, Y. 2004, MNRAS, 353, 689
- Kervella, P., Thévenin, F., Di Folco, E., Ségransan, D. 2004 A&A 426, 297
- Kovács, G., Zucker, S., Mazeh, T., 2002 A&A 391. 369
- Lister, T.A., West, R.G., Wilson, D.M., Collier Cameron, A., Clarkson, W.I., Street, R., Enoch, B., Parley, N.R., Christian, D.J., Kane, S.R., Evans, A., Fitzsimmons, A., Haswell, C.A., Hellier, C., Hodgkin, S., Horne, K.D., Irwin, J., Keenan, F.P., Norton, A.J., Osborne, J., Pollacco, D.L., Ryans, R., Skillen, I., Wheatley, P.J., Barnes, J.R., 2007 MNRAS accepted, astro-ph/0705.2603
- Mayor, M. & Queloz, D. 1995, Nature, 378, 355
- McCullough, P.R., Stys, J. E., Valenti, Jeff A., Johns-Krull, C. M., Janes, K. A., Heasley, J. N., Bye, B. A., Dodd, C., Fleming, S. W., Pinnick, A., Bissinger, R., Gary, B. L., Howell, P. J., Vanmunster, T., 2006 ApJ 648, 1228
- Monet, D.G., Levine, S. E.; Canzian, B.; Ables, H. D.; Bird, A. R.; Dahn, C. C.; Guetter, H. H.; Harris, H. C.; Henden, A. A.; Leggett, S. K.; Levison, H. F.; Luginbuhl, C. B.; Martini, J.; Monet, A. K. B.; Munn, J. A.; Pier, J. R.; Rhodes, A. R.; Rieke, B.; Sell, S.; Stone, R.C.; Vrba, F. J.; Walker, R. L.; Westerhout, G.; Brucato, R. J.; Reid, I. N.; Schoening, W.; Hartley, M.; Read, M. A.; Tritton, S. B., 2003 AJ 125, 984
- Moutou, C., Loeillet, B., Bouchy, F., da Silva, R., Mayor, M., Pont, F., Queloz, D., Santos, N. C., Sággransan, D., Udry, S., Zucker, S., 2006 A&A 458, 327
- Nikolaev, S. Weinberg, M. D., Skrutskie, M.F., Cutri, R. M., Wheelock, S.L., Gizis, J.E., Howard, E.M.. 2000 AJ 120, 3340
- Pollacco, D.L., Skillen, I., Cameron, A. Collier, Christian, D. J., Hellier, C., Irwin, J., Lister, T. A., Street, R. A., West, R. G., Anderson, D., Clarkson, W. I., Deeg, H., Enoch, B., Evans, A., Fitzsimmons, A., Haswell, C. A., Hodgkin, S., Horne, K., Kane, S. R., Keenan, F. P., Maxted, P. F. L., Norton, A. J., Osborne, J., Parley, N. R., Ryans, R. S. I., Smalley, B., Wheatley, P. J., Wilson, D. M., 2006 PASP 118, 1407
- Pollack, J.B., Hubickyj, O., Bodenheimer, P., Lissauer, J.J., Podolak, M., Greenzweig, Y., 1996 Icarus 124,62
- Pont, F., Zucker, S., Queloz, D., 2006 MNRAS 373, 231
- Richardson, L.J., Deming D. & Seager, S. 2003 ApJ 597, 581
- Sahu, K.C., Casertano, S., Bond, H.E., Valenti, J., Smith, T.Ed., Minniti, D., Zoccali, M., Livio, M., Panagia, N., Piskunov, N., Brown, T.M., Brown, T., Renzini, A., Rich, R. M., Clarkson, W.I., Lubow, S. 2006 Nature 443, 534
- Sirko, E. & Paczyński 2003 ApJ 592, 1217
- Smith, A.M.S., Collier Cameron, A., Christian, D. J., Clarkson, W. I., Enoch, B., Evans, A., Haswell, C. A., Hellier, C., Horne, K., Irwin, J., Kane, S. R., Lister, T. A., Norton, A. J., Parley, N., Pollacco, D. L., Ryans, R., Skillen, I., Street, R. A., Triaud, A. H. M. J., West, R. G.,



- Wheatley, P. J., Wilson, D. M., 2006 MNRAS 373, 1151  
Stetson, P.B., 1990 PASP 102, 932  
Street, R.A., Horne, Keith, Lister, T. A., Penny, A. J., Tsapras, Y., Quirrenbach, A., Safizadeh, N., Mitchell, D., Cooke, J., Collier Cameron, A. 2003 MNRAS 340, 1287  
Street, R.A., Christian, D.J., Clarkson, W.I., Collier Cameron, A., Enoch, B., Kane, S.R., Lister, T.A., West, R.G., Wilson, D.M., Evans, A., Fitzsimmons, A., Haswell, C.A., Hellier, C., Hodgkin, S.T., Horne, K.D., Irwin, J., Keenan, F.P., Norton, A.J., Osborne, J., Pollacco, D.L., Ryans, R., Skillen, I., Wheatley, P.J., Barnes, J., 2007 MNRAS accepted, astro-ph/0705.2598  
Tamuz, O., Mazeh, T., Zucker, S., 2005 MNRAS 356, 1466  
Tingley, B., Sackett, P.D., 2005 ApJ 627, 1011  
Udalski, A., Paczynski, B., Zebrun, K., Szymanski, M., Kubiak, M., Soszynski, I., Szewczyk, O., 2002a, Acta Astron., 52, 1  
Udalski, A., Zebrun, K., Szymanski, M., Kubiak, M., Soszynski, I., Szewczyk, O., Wyrzykowski, L., Pietrzynski, G., 2002b, Acta Astron., 52, 115  
Udalski, A., Szewczyk, O., Zebrun, K., Pietrzynski, G., Szymanski, M., Kubiak, M., Soszynski, I., Wyrzykowski, L., 2002c, Acta Astron., 52, 317  
Udry, S., Mayor, M., Naef, D., Pepe, F., Queloz, D., Santos, N. C., Burnet, M., Confino, B., Melo, C. 2000 A&A 356, 590  
Valenti, J. A., Fisher, D.A., 2005 ApJS 159, 141  
Vidal-Madjar, A., Désert, J.-M., Lecavelier des Etangs, A., Hébrard, G., Ballester, G. E., Ehrenreich, D., Ferlet, R., McConnell, J. C., Mayor, M., Parkinson, C. D., 2004 ApJ 604, L69  
Wilson D.M., Enoch, B., Christian, D. J., Clarkson, W. I., Collier Cameron, A., Deeg, H. J., Evans, A., Haswell, C. A., Hellier, C., Hodgkin, S. T., Horne, K., Irwin, J., Kane, S. R., Lister, T. A., Maxted, P. F. L., Norton, A. J., Pollacco, D., Skillen, I., Street, R. A., West, R. G., Wheatley, P. J., 2006, Proceedings of the Transiting Extrasolar Planets Workshop, Heidelberg, ASP Conf. Ser. 118, 1245  
Worley, C. E. & Douglass, G. G., 1997 A&AS 125, 523  
Zombeck, M.V., 1992, *Handbook of Space Astronomy and Astrophysics*, 1992, Knudsen